© 2020. Published by The Company of Biologists Ltd | Journal of Cell Science (2020) 133, jcs234047. doi:10.1242/jcs.234047

RESEARCH ARTICLE

CLN3 regulates endosomal function by modulating Rab7A–effector interactions

Seda Yasa[1], Graziana Modica[1], Etienne Sauvageau[1], Abuzar Kaleem[2], Guido Hermey[2] and Stephane Lefrancois[1,3,4,*]

ABSTRACT

Mutations in *CLN3* are a cause of juvenile neuronal ceroid lipofuscinosis (JNCL), also known as Batten disease. Clinical manifestations include cognitive regression, progressive loss of vision and motor function, epileptic seizures and a significantly reduced lifespan. CLN3 localizes to endosomes and lysosomes, and has been implicated in intracellular trafficking and autophagy. However, the precise molecular function of CLN3 remains to be elucidated. Previous studies showed an interaction between CLN3 and Rab7A, a small GTPase that regulates several functions at late endosomes. We confirmed this interaction in live cells and found that CLN3 is required for the efficient endosome-to-TGN trafficking of the lysosomal sorting receptors because it regulates the Rab7A interaction with retromer. In cells lacking CLN3 or expressing CLN3 harbouring a disease-causing mutation, the lysosomal sorting receptors were degraded. We also demonstrated that CLN3 is required for the Rab7A–PLEKHM1 interaction, which is required for fusion of autophagosomes to lysosomes. Overall, our data provide a molecular explanation behind phenotypes observed in JNCL and give an indication of the pathogenic mechanism behind Batten disease.

This article has an associated First Person interview with the first author of the paper.

KEY WORDS: Endosomes, CLN3, Retromer, Sortilin, Juvenile neuronal ceroid lipofuscinosis, Rab7A

INTRODUCTION

The neuronal ceroid lipofuscinoses (NCLs) are a group of rare neurodegenerative diseases linked to over 430 mutations in 13 genetically distinct genes (*CLN1–CLN8* and *CLN10–CLN14*) (Mole and Cotman, 2015). Clinical manifestations of NCLs include intellectual impairment, progressive loss of vision and motor function, epileptic seizures and a significantly reduced lifespan (Anderson et al., 2012). At the cellular level, NCLs display aberrant lysosomal function and an excessive accumulation of ceroid lipofuscin in neurons as well as other cell types outside of the central nervous system (Anderson et al., 2012).

[1]Centre Armand-Frappier Santé Biotechnologie, Institut National de la Recherche Scientifique, Laval, Canada H7V 1B7. [2]Institute for Molecular and Cellular Cognition, Center for Molecular Neurobiology Hamburg, University Medical Center Hamburg-Eppendorf, 20251 Hamburg, Germany. [3]Department of Anatomy and Cell Biology, McGill University, Montreal, Canada H3A 0C7. [4]Centre d'Excellence en Recherche sur les Maladies Orphelines - Fondation Courtois (CERMO-FC), Université du Québec à Montréal (UQAM), Montréal, Canada H2X 3Y7.

*Author for correspondence (stephane.lefrancois@iaf.inrs.ca)

S.L., 0000-0002-3312-9594

Received 10 May 2019; Accepted 22 January 2020

Juvenile neuronal ceroid lipofuscinosis (JNCL) is caused by germline mutations in ceroid lipofuscinosis neuronal-3 (CLN3). More often referred to as Batten disease, it is the most common paediatric neurodegenerative disease (Anderson et al., 2012; Mole and Cotman, 2015). CLN3 is a protein of 438 amino acids with six transmembrane domains whose N- and C-terminal ends are located in the cytosol (Ratajczak et al., 2014). The most common mutation results in the deletion of exon 7 and 8 ($CLN3^{\Delta ex7–8}$), but several other mutations have been identified (Cotman and Staropoli, 2012). CLN3 is a highly glycosylated integral membrane protein (Storch et al., 2004) that localizes to the endosomal/lysosomal membrane (Oetjen et al., 2016) among other intracellular locations and has proposed roles in lysosomal trafficking and autophagy (Lojewski et al., 2014; Metcalf et al., 2008). CLN3 interacts with and has been implicated in Rab7A recruitment to endosomal membranes (Luiro et al., 2004; Uusi-Rauva et al., 2012); however, the function of this interaction is unknown. Furthermore, how disease-causing mutations in CLN3 affect this interaction or the downstream functions of Rab7A has not been elucidated.

The Ras-like proteins in brain (Rabs) are key regulators of the formation, trafficking, and fusion of transport vesicles at the endoplasmic reticulum (ER), Golgi apparatus and early and late endosomes (Hutagalung and Novick, 2011). Rabs function by interacting with downstream effectors (Grosshans et al., 2006) and a key process regulating these interactions is the GTP loading or 'activation' of Rab GTPases at specific membrane sites (Pfeffer and Aivazian, 2004). This GDP to GTP switch is regulated by guanine exchange factors (GEFs) that load Rab GTPases with GTP, while GTPase activating proteins (GAPs) terminate their activity by hydrolysing the GTP to GDP (Barr and Lambright, 2010).

Active GTP-loaded Rab7A localizes to endosomal membranes and recruits numerous effectors to perform a variety of functions such as endosome-to-trans Golgi network (TGN) trafficking (Rojas et al., 2008; Seaman et al., 2009), autophagosome–lysosome fusion (McEwan et al., 2015), lysosomal positioning (Wijdeven et al., 2016) and degradation of endocytic cargo, such as epidermal growth factor (EGF) receptor (EGFR) (Vanlandingham and Ceresa, 2009).

In this study, we systematically analysed several of these Rab7A-mediated pathways to determine which was under the control of CLN3. We identified defects in endosome-to-TGN sorting and EGFR degradation. Overall, our data suggest a role for CLN3 as a regulator of Rab7A function. Our data provide insight into the possible pathogenic mechanism in Batten disease.

RESULTS

A subset of disease-causing mutations in CLN3 alters its interactions

It has been reported that CLN3 interacts with the small GTPase Rab7A (Uusi-Rauva et al., 2012), but the functional role of this

Journal of Cell Science (2020) 133, jcs234047. doi:10.1242/jcs.234047

interaction is not understood and it is not clear how disease-causing mutations in CLN3 affect this interaction. We used bioluminescence resonance energy transfer (BRET) to confirm the CLN3–Rab7A interaction in live cells and to determine how disease-causing mutations affect this interaction. Compared with co-immunoprecipitation, BRET is performed in live cells, with proteins localized to their native environment. From BRET titration curves, the $BRET_{50}$ can be calculated which is the value at which the concentration of the acceptor is required to obtain 50% of the maximal BRET signal ($BRET_{MAX}$) and is indicative of the propensity of the protein pair to interact (Kobayashi et al., 2009; Mercier et al., 2002). The smaller the $BRET_{50}$, the stronger the interaction. Renilla luciferase II (RlucII) was fused at the N-terminus to wild-type Rab7A (RlucII-Rab7A). As previously shown, this tag had little effect on the distribution or function of Rab7A, as expressing RlucII-Rab7A in Rab7A-knockout cells (Rab7A-KO) rescued retromer recruitment (Modica et al., 2017). The energy acceptor green fluorescent protein 10 (GFP10) was fused to the N-terminus of wild-type and various CLN3 mutants (GFP10-CLN3, GFP10-$CLN3^{R334H}$, GFP10-$CLN3^{V330F}$, GFP10-$CLN3^{E295K}$, GFP10-$CLN3^{L101P}$). These mutations have been previously studied and were shown to localize to late endosomes/lysosomes similarly to wild-type CLN3 (Haskell et al., 2000). We engineered a CLN3 mutant harbouring the common exon 7 and 8 deletion ($CLN3^{\Delta ex7–8}$), but we could not efficiently express this protein in our lab. HeLa cells were co-transfected with a constant amount of RlucII-Rab7A and increasing amounts of GFP10-CLN3 to generate BRET titration curves. The BRET signal between RlucII-Rab7A and GFP10-CLN3 rapidly increased with increasing amounts of expressed GFP10-CLN3 until it reached saturation, suggesting a specific interaction (Fig. 1A, blue curve). We also tested another Rab GTPase, Rab1a, which is localized to the Golgi (Dumaresq-Doiron et al., 2010), to confirm the specificity of the CLN3–Rab7A interaction. We generated BRET titration curves with RlucII-Rab1a (Fig. 1A, red curve) in HeLa cells. We extrapolated the $BRET_{50}$ for the interaction between CLN3 and the two Rab GTPases and found that the Rab7A–CLN3 interaction had a much smaller $BRET_{50}$ (0.004) compared with the value (0.020) for the Rab1a–CLN3 interaction, indicating that Rab7A has a higher propensity to interact with CLN3 compared with Rab1a (Fig. 1B). A small fraction of CLN3 localizes to the Golgi (Cao et al., 2006), hence we were not surprised to detect an interaction between CLN3 and Rab1a. Next, we tested the interaction between CLN3 and $Rab7A^{C205,207S}$, which is a mutant form of Rab7A that cannot be recruited to membranes owing to its lack of prenylation (Modica et al., 2017). We found no interaction between $Rab7A^{C205,207S}$ and CLN3 (Fig. 1A, green line). Finally, we tested if the small GTPase Arf6 can interact with CLN3 (Fig. 1A, orange line) and found no interaction, indicating that the signal we observed between Rab7a and CLN3 is due to a specific interaction between the two proteins. We next performed a BRET experiment to determine the impact of CLN3 disease-causing mutations on the CLN3–Rab7A interaction (Fig. 1C). Compared with wild-type CLN3, we found a significantly stronger (smaller $BRET_{50}$) interaction between Rab7A and $CLN3^{R334H}$ or $CLN3^{V330F}$ (Fig. 1D), whereas the $CLN3^{E295K}$ and $CLN3^{L101P}$ mutations had negligible effects on the CLN3–Rab7A interaction (Fig. 1D). To confirm our BRET data, we tested these interactions via co-immunoprecipitation (co-IP). We expressed FLAG-tagged wild-type CLN3 and the various CLN3 mutants in HeLa cells, immunoprecipitated the various forms of CLN3 with anti-FLAG antibody and blotted for endogenous Rab7A. By co-IP, we confirmed the CLN3–Rab7A interaction and found that only $CLN3^{L101P}$ did not interact with Rab7A (Fig. S1A).

Mutations in CLN5, which interacts with CLN3, cause a form of NCL with overlapping symptoms to CLN3 disease (Vesa et al., 2002). In our previous work, we showed that CLN5 interacts with sortilin (also known as SORT1) (Mamo et al., 2012). Therefore, we rationalized that CLN3 could also interact with this lysosomal sorting receptor. To test this hypothesis, we performed a BRET experiment by expressing a constant amount of RlucII-tagged wild-type CLN3 (RlucII-CLN3) and increasing amounts of yellow fluorescence protein (YFP) tagged sortilin. We found an interaction between CLN3 and sortilin, as the curve reached saturation (Fig. 1E, blue curve). We next determined the impact CLN3 disease-causing mutations could have on this interaction. We generated BRET titration curves between sortilin-YFP and RlucII-$CLN3^{R334H}$ (Fig. 1E, red curve), RlucII-$CLN3^{V330F}$ (Fig. 1E, green curve), RlucII-$CLN3^{E295K}$ (Fig. 1E, black curve) and RlucII-$CLN3^{L101P}$ (Fig. 1E, purple curve). As a control, we used Sigma-1 receptor (S1R-YFP), a type I integral membrane protein also known as SIGMAR1 (Fig. 1E, orange line) (Prause et al., 2013). We found no interaction between CLN3 and Sigma-1 receptor. Compared with wild-type CLN3, we found a significant increase in the $BRET_{50}$ values for the sortilin–$CLN3^{E295K}$ and sortilin–$CLN3^{L101P}$ interactions, suggesting weaker interactions (Fig. 1F). Interestingly, we found no change in the sortilin–$CLN3^{R334H}$ and sortilin–$CLN3^{V330F}$ interactions compared with the sortilin–CLN3 interaction (Fig. 1F). To confirm these BRET results by co-IP, we expressed FLAG-tagged wild-type CLN3 and the various CLN3 mutants in HeLa cells, immunoprecipitated the various forms of CLN3 with anti-FLAG antibody, and blotted for endogenous sortilin. We found that $CLN3^{L101P}$ had a significant negative impact on the CLN3–sortilin, which is consistent with our BRET data (Fig. S1A).

CLN3 is not required for the steady-state membrane distribution of Rab7A

A previous study had found that Rab7A immunofluorescence staining was decreased in cells harbouring the homozygous mutation ($CLN3^{\Delta ex7–8}$/$CLN3^{\Delta ex7–8}$) compared with wild-type cells (Fossale et al., 2004). Based on this, we investigated whether CLN3 is required for the membrane recruitment of Rab7A by generating CLN3-KO HeLa cells using CRISPR/Cas9 (Fig. S2A). We also generated Rab7A-KO cells using the same parental HeLa strain to serve as a control in our experiments (Fig. S2B). Previous work has demonstrated that cells harbouring CLN3 mutations accumulate LC3II-positive autophagosomes (Fossale et al., 2004; Vidal-Donet et al., 2013). Soluble microtubule-associated protein 1A/1B-light chain 3 (LC3; also known as MAP1LC3B) forms LC3-II through lipidation upon activation of autophagy. LC3-II then localizes to autophagosomal membranes and remains there until autophagosomes fuse with lysosomes, resulting in its degradation (Ganley et al., 2011). If autophagosome–lysosome fusion is inhibited, or if lysosomal function is blocked, either by a compound such as bafilomycin A1 (BafA1) or a defective protein, degradation of LC3-II cannot occur. Therefore, comparing the turnover of LC3-II levels is a good measure of autophagic activity and competence. To test if our CLN3-KO cells behaved as expected with respect to autophagy, we initiated autophagy through nutrient starvation by incubating wild-type, CLN3-KO and Rab7A-KO cells in the presence or absence of BafA1. We found an increase in the LC3-II/total LC3 ratio in wild-type cells upon starvation compared with fed conditions, which was further increased in BafA1-treated cells (Fig. S2C,D) suggesting that wild-type HeLa cells could initiate LC3 recruitment and degrade it, unless lysosomal function was inhibited pharmacologically. Next, we

Journal of Cell Science (2020) 133, jcs234047. doi:10.1242/jcs.234047

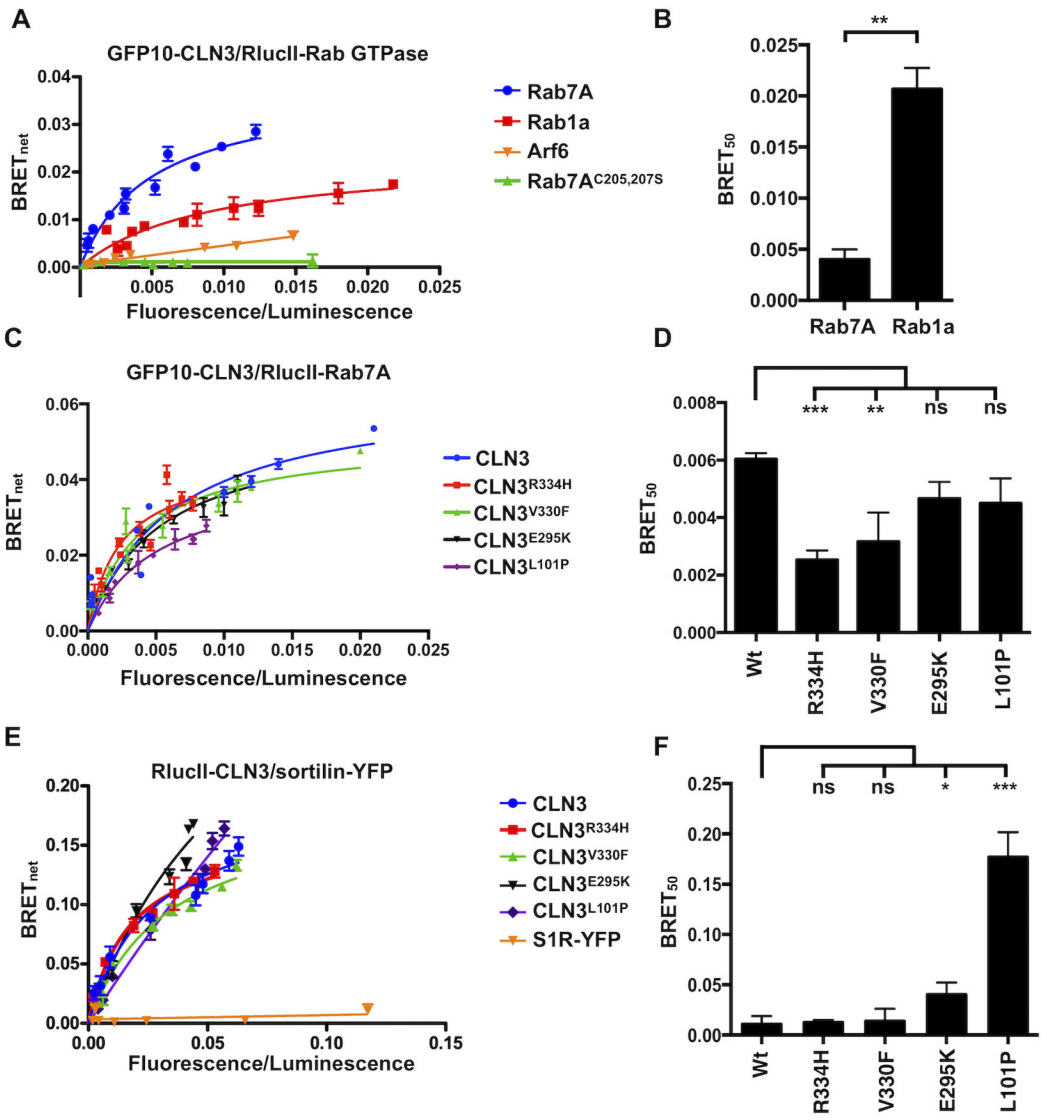

Fig. 1. CLN3 interacts with Rab7A and sortilin. (A) HeLa cells were transfected with a constant amount of RlucII-Rab7A (blue curve), RlucII-Rab1a (red curve), Arf6-RlucII (orange line) or RlucII-Rab7A^{C205,207S} (green line) and increasing amounts of GFP10-CLN3 to generate BRET titration curves. 48 h post-transfection, BRET analysis was performed. BRET signals are plotted as a function of the ratio between the GFP10 fluorescence over RlucII luminescence. (B) $BRET_{50}$ was extrapolated from three independent experiments. (C) HeLa cells were transfected with a constant amount of RlucII-Rab7A and increasing amounts of GFP10-CLN3, GFP10-CLN3^{R334H}, GFP10-CLN3^{V330F}, GFP10-CLN3^{E295K} or GFP10-CLN3^{L101P} to generate BRET titration curves. $BRET_{MAX}$, maximal BRET signal. (D) $BRET_{50}$ was extrapolated from three independent experiments. (E) HeLa cells were transfected with a constant amount of RlucII-CLN3 or RlucII-CLN3 harbouring a disease-causing mutation and increasing amounts of sortilin-YFP or Sigma-1 receptor-YFP (S1R-YFP) to generate BRET titration curves. 48 h post-transfection, BRET analysis was performed. BRET signals are plotted as a function of the ratio between the YFP fluorescence over RlucII luminescence. (F) $BRET_{50}$ was extrapolated from three independent experiments. Data are mean±s.d.; ns, not significant; *P≤0.05; **P≤0.01; ***P≤0.001; two-way ANOVA followed by Tukey's *post hoc* test in D and F; Student's *t*-test in B.

used Rab7A-KO HeLa cells as a control group, since without Rab7A, we would expect defects in LC3 degradation and therefore a higher ratio of LC3-II/total LC3 (Fig. S2C,D). As expected, we found a higher basal level of LC3-II/total LC3 levels, which increased upon the induction of autophagy. The addition of BafA1 did not increase this ratio (Fig. S2C,D), suggesting a defect in late stages of autophagy in Rab7A-KO cells as expected. In CLN3-KO HeLa cells, we observed a higher LC3-II/total LC3 ratio compared with wild-type cells. Much like Rab7A-KO cells, the LC3-II/Total LC3 ratio increased in starvation conditions, and was not increased further by BafA1 treatment (Fig. S2C,D). Overall, our data from the CLN3-KO HeLa cells support previously published results suggesting that cells lacking CLN3 are defective in late stages of autophagy. Combined with our sequencing data, this confirms ablation of CLN3 in this cell line.

To determine if CLN3 is required for the membrane recruitment of Rab7A, we performed a membrane isolation technique that we have used previously (Mamo et al., 2012; Modica et al., 2017), in wild-type, CLN3-KO and CLN3-KO HeLa cells expressing FLAG-CLN3 (Fig. 2A). Our membrane separation was successful, as the integral membrane protein Lamp2 was found in the pellet fraction (P), while the cytosolic protein tubulin was found in the supernatant fraction (S) (Fig. 2A). Quantification of 5 independent experiments showed that Rab7A was not significantly displaced from membranes to the cytosolic fraction in CLN3-KO HeLa cells compared with wild-type HeLa cells, while the expression of Flag-

Journal of Cell Science (2020) 133, jcs234047. doi:10.1242/jcs.234047

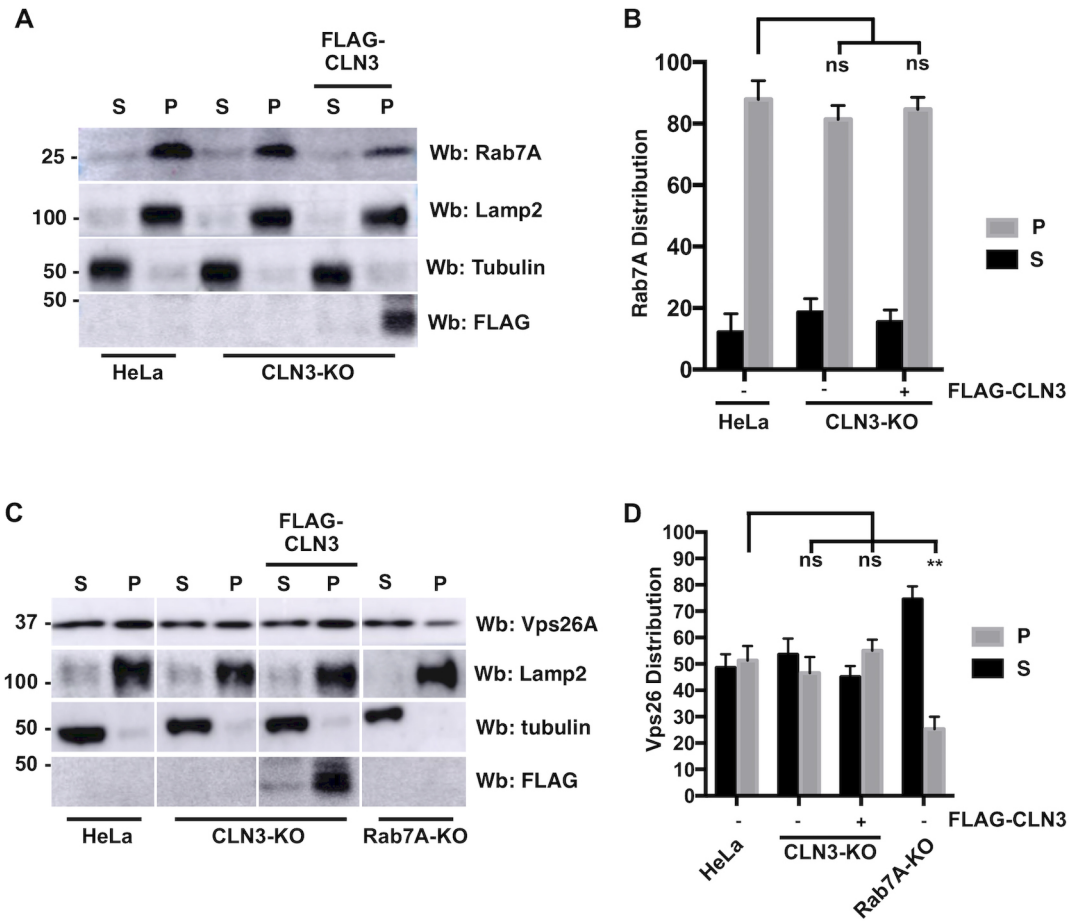

Fig. 2. CLN3 is not required for the recruitment of Rab7A to membrane. Wild-type, CLN3-KO and FLAG-CLN3 expressing CLN3-KO HeLa cells were collected for membrane isolation assay. Samples were subjected to western blotting with anti-Rab7A antibody, anti-Lamp2 antibody (a marker for the membrane fraction) and anti-tubulin antibody (a marker for the cytosolic fraction). Anti-FLAG staining shows the expression of wild-type CLN3 rescue. S, supernatant, P, pellet. (B) Quantification of 5 separate membrane isolation assay experiments. (C) Wild-type, CLN3-KO, FLAG-CLN3 expressing CLN3-KO and Rab7A-KO HeLa cells were collected for a membrane isolation assay. After the isolation, samples were subjected to western blotting with anti-Vps26A antibody (a retromer subunit), anti-Lamp2 antibody and anti-tubulin antibody. Anti-FLAG staining shows expression of wild-type CLN3. S, supernatant, P, pellet. (D) Quantification of 5 separate membrane isolation assay experiments. Data in B and D are mean±s.d. ns, not significant; $^{**}P \leq 0.01$; two-way ANOVA followed by Tukey's *post hoc* test.

CLN3 in CLN3-KO cells did not affect this phenotype (Fig. 2B). The small GTPase Rab7A regulates the spatiotemporal recruitment of retromer (Rojas et al., 2008; Seaman et al., 2009), a protein complex required for efficient endosome-to-TGN traffic of cation-independent mannose 6-phosphate receptor (CI-MPR; also known as IGF2R) and sortilin (Arighi et al., 2004; Canuel et al., 2008b; Seaman, 2004). In cells lacking retromer, these receptors do not efficiently recycle to the TGN, accumulate at late endosomes and are subsequently degraded in lysosomes (Arighi et al., 2004; Seaman, 2004). However, in Rab7A-depleted cells, CI-MPR was not efficiently recycled to the TGN, but was not degraded either (Rojas et al., 2008). We repeated the membrane assay as above, but we included Rab7A-KO HeLa cells as a control, as we previously demonstrated a reduction of retromer recruitment in Rab7A-KO HEK293 cells (Modica et al., 2017). Lamp2 and tubulin were used as markers of membrane (P) and cytosolic fractions (S), respectively (Fig. 2C). Compared with wild-type HeLa cells, we observed a significant decrease in retromer recruitment (as detected by staining with the retromer subunit Vps26A) in Rab7A-KO HeLa cells, but we did not observe any significant changes in CLN3-KO cells (Fig. 2C). Quantification from 3 independent experiments found no changes in the membrane distribution of retromer in CLN3-KO and CLN3-KO cells expressing FLAG-CLN3 compared with wild-type cells (Fig. 2D). However, we found a 26% increase of retromer in the supernatant (cytosolic fraction) of Rab7A-KO cells compared with wild-type cells (Fig. 2D), which is comparable to other previously published studies (Mamo et al., 2012; Seaman et al., 2009).

CLN3 is required for efficient retromer interactions

Although we found no defects in the membrane distribution of retromer in CLN3-KO cells, we wondered if we could observe other changes. Rab7A interacts with retromer, which is required for the spatiotemporal recruitment of the latter. We tested whether or not the interaction between Rab7A and retromer is affected in CLN3-KO cells. We have previously used BRET to study the Rab7A–Vps26A interaction (Modica et al., 2017). This interaction is specific as Rab7A did not interact with AP-1 subunits (a clathrin adaptor that has been localized to both the TGN and endosomes), whereas Vps26A did not interact with Rab1a (Modica et al., 2017). First, we investigated whether Vps26A-GFP10 could be part of the retromer trimer. We found that endogenous Vps35 could co-immunoprecipitate with both wild-type Vps26A and Vps26A-GFP10, suggesting the GFP10-tagged protein could be included in

Journal of Cell Science (2020) 133, jcs234047. doi:10.1242/jcs.234047

the retromer trimer (Fig. S3A). Next, we generated BRET titration curves between RlucII-Rab7A and Vps26A-GFP10 in wild-type (blue curve) and CLN3-KO (red curve) HeLa cells (Fig. 3A). Compared with wild-type HeLa cells, we found a twofold increase in the $BRET_{50}$ values for Rab7A binding to Vps26A in CLN3-KO cells, suggesting a weaker interaction (Fig. 3B). As a control, we tested the Rab1a–Vps26A interaction in HeLa cells. We found no interaction between Rab1a and Vps26A in wild-type HeLa cells (Fig. 3A, green line). We previously demonstrated that the retromer–Rab7A interaction requires the palmitoylation of Rab7A (Modica et al., 2017). We tested whether the palmitoylation level of Rab7A was lower in CLN3-KO versus wild-type HeLa cells using Acyl-RAC, a technique to determine the palmitoylation status of a protein (Fig. 3C). Quantification of three separate Acyl-RAC assays found no significant change in the level of palmitoylation of Rab7A in CLN3-KO cells compared with wild-type HeLa cells (Fig. 3D). As we observed no changes in the palmitoylation level of Rab7A in CLN3-KO cells, we next tested if the GTP loading of Rab7A was affected in CLN3-KO, using a well-characterized FRET biosensor (Yasuda et al., 2016). We found no differences in the GTP loading of Rab7A between wild-type and CLN3-KO HeLa cells (Fig. 3E), suggesting that CLN3 does not alter the GTP loading of Rab7A.

We next asked if CLN3 can interact with retromer. We generated BRET titration curves using RlucII-CLN3 and Vps26A-GFP10 (Fig. 4A, blue curve). As a control, we tested whether or not retromer can interact with ABCD4, a multi-spanning integral membrane protein localized to endolysosomes (Coelho et al., 2012). We identified an interaction between CLN3 and retromer (Fig, 4A, blue curve), but not between ABCD4 and retromer (Fig. 4A, orange line). Although the signal increases rapidly, suggesting numerous random collisions, the signal does not saturate, suggesting no interaction. The $CLN3^{R334H}$ (Fig. 4A, red curve) and $CLN3^{E295K}$

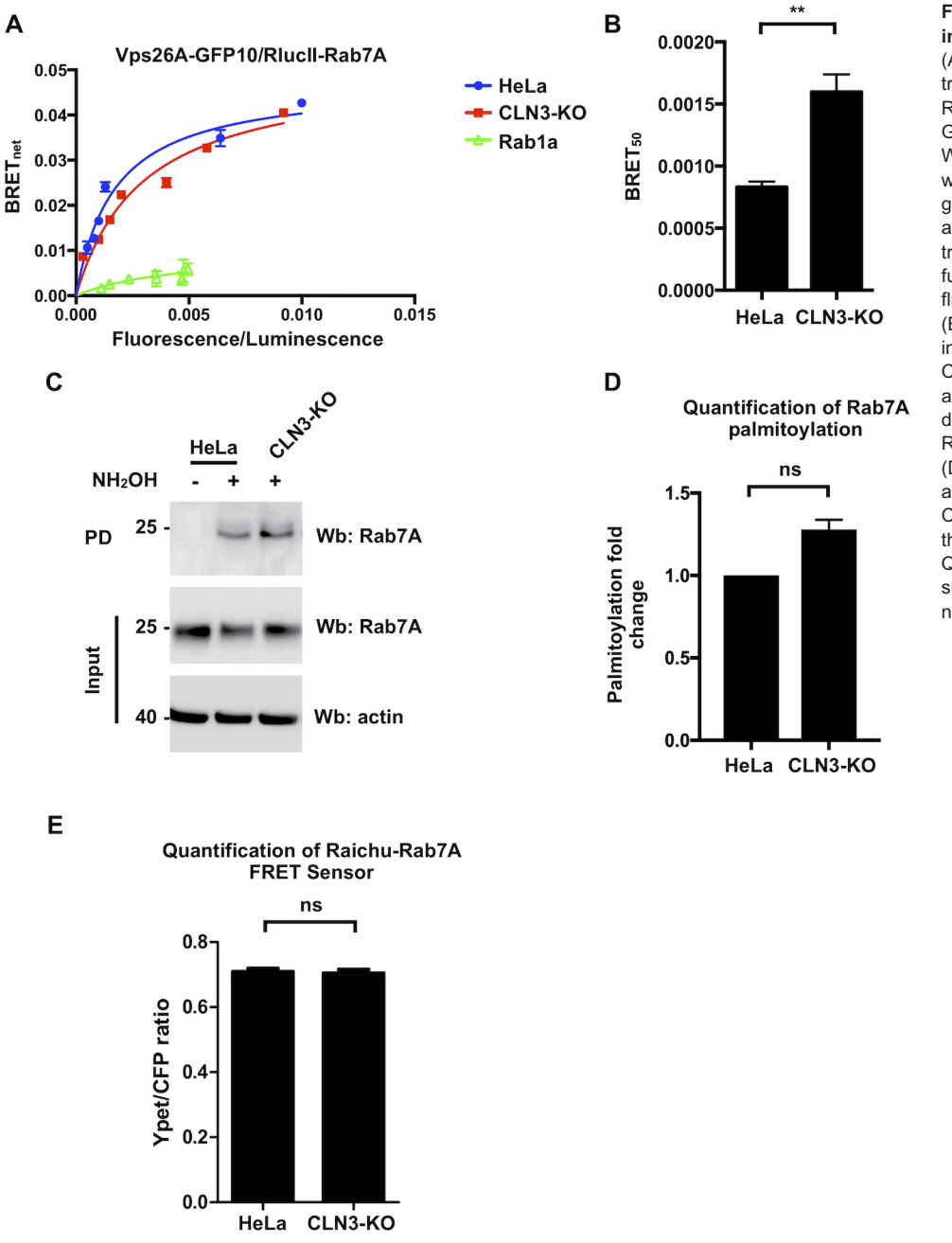

Fig. 3. CLN3 is required for the efficient interaction of Rab7A with retromer. (A) Wild-type and CLN3-KO HeLa cells were transfected with a constant amount of RlucII-Rab7A and increasing amounts of Vps26A-GFP10 to generate BRET titration curves. Wild-type HeLa cells were also transfected with RlucII-Rab1a and Vps26A-GFP10 to generate BRET titration curves. BRET analysis was performed 48 h post-transfection. BRET signals are plotted as a function of the ratio between the GFP10 fluorescence over RlucII luminescence. (B) $BRET_{50}$ was extrapolated from 3 independent experiments. (C) Wild-type and CLN3-KO HeLa cell lysates were collected and subjected to Acyl-RAC analysis to determine the palmitoylation status of Rab7A. NH_2OH: Hydroxylamine. (D) Quantification of 3 separate Acyl-RAC assay experiments. (E) Wild-type and CLN3-KO HeLa cells were transfected with the FRET sensor, Raichu-Rab7A. Quantification of 4 separate experiments are shown. Data in B, D and E are mean±s.d. ns, not significant; $^{**}P \leq 0.01$; Student's *t*-test.

Journal of Cell Science (2020) 133, jcs234047. doi:10.1242/jcs.234047

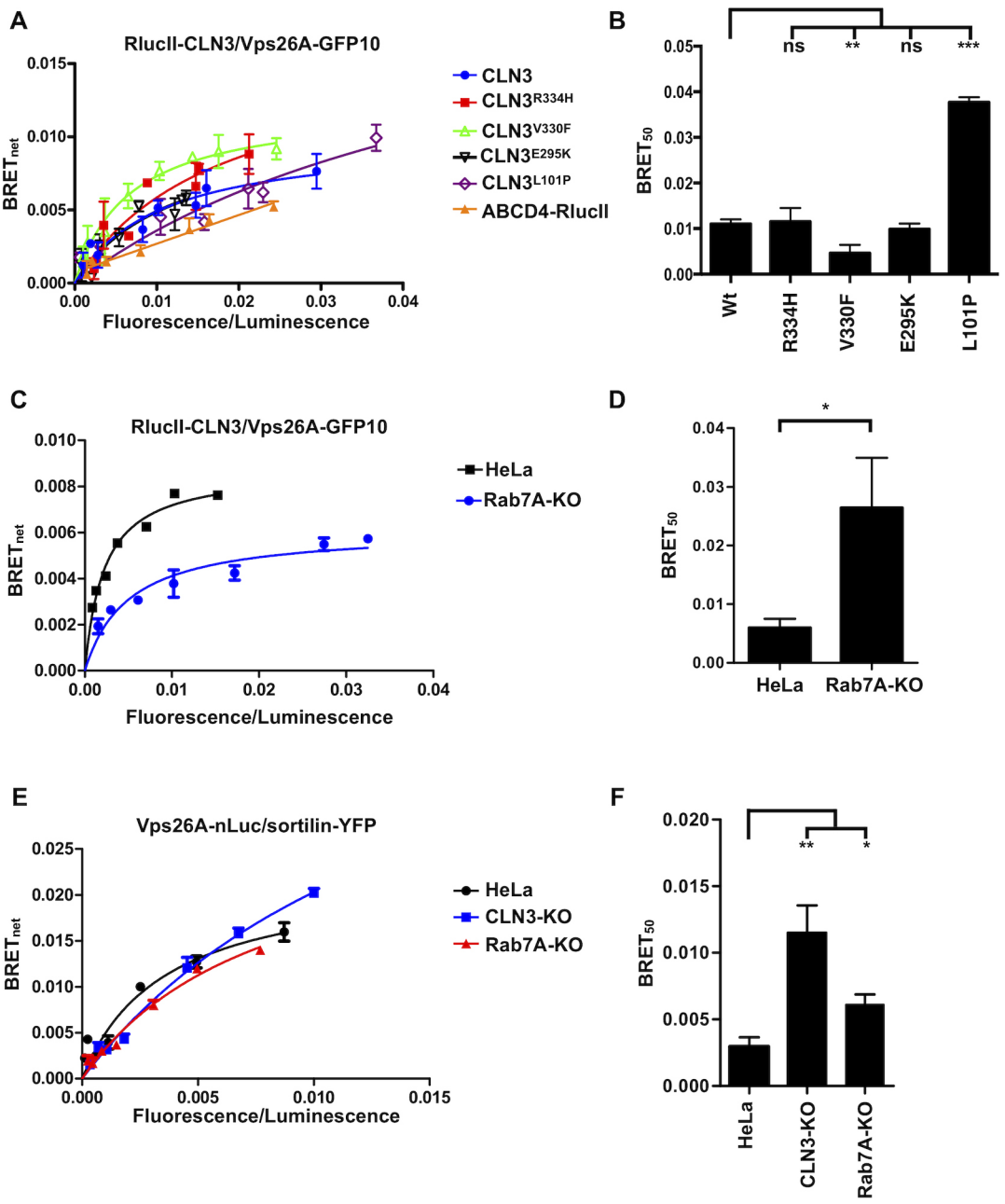

Fig. 4. CLN3 interacts with retromer and modulates the sortilin–retromer interaction. (A) HeLa cells were transfected with a constant amount of RlucII-CLN3, RlucII-CLN3 harbouring a disease-causing mutation or ABCD4-RlucII and increasing amounts of Vps26A-GFP10 to generate BRET titration curves. BRET analysis was performed 48 h post-transfection. BRET signals are plotted as a function of the ratio between the GFP10 fluorescence over RlucII luminescence. (B) $BRET_{50}$ was extrapolated from 3 independent experiments. (C) Wild-type and Rab7A-KO HeLa cells were transfected with a constant amount of RlucII-CLN3 and increasing amounts of Vps26A-GFP10 to generate BRET titration curves. 48 h post-transfection BRET analysis was performed. BRET signals are plotted as a function of the ratio between the GFP10 fluorescence over RlucII luminescence. (D) BRET50 was extrapolated from 4 independent experiments. (E) Wild-type, CLN3-KO and Rab7A-KO HeLa cells were transfected with a constant amount of Vps26A-nLuc and increasing amounts of sortilin-YFP to generate BRET titration curves. BRET analysis was performed 48 h post-transfection. BRET signals are plotted as a function of the ratio between the YFP fluorescence over nLuc luminescence. (F) $BRET_{50}$ was extrapolated from 3 independent experiments. Data are mean±s.d. ns, not significant; *$P \leq 0.05$; **$P \leq 0.01$; two-way ANOVA followed by Tukey's *post hoc* test in B and F; Student's *t*-test in D.

(Fig. 4A, black curve) mutations had no impact on this interaction (Fig. 4B). Interestingly, the $CLN3^{V330F}$ (Fig. 4A, green curve) increased the propensity of CLN3 to interact with retromer, whereas the $CLN3^{L101P}$ mutation (Fig. 4A, purple curve), significantly weakened the interaction (Fig. 4B). We again used co-immunoprecipitation to confirm these BRET results and found that endogenous Vps26A was able to efficiently interact with all forms of FLAG-tagged CLN3 except $CLN3^{L101P}$, confirming our BRET data (Fig. S1A).

We next aimed to determine if the CLN3–retromer interaction was dependent on Rab7A. We generated BRET titration curves between RlucII-CLN3 and Vps26A-GFP10 in wild-type (Fig. 4C, black curve) and Rab7A-KO (Fig. 4C, blue curve) HeLa cells. We found a significantly weaker CLN3–retromer interaction in Rab7A-KO

Journal of Cell Science (2020) 133, jcs234047. doi:10.1242/jcs.234047

compared with wild-type HeLa cells. CI-MPR and sortilin are known to interact with retromer, which is necessary for their endosome-to-TGN trafficking (Arighi et al., 2004; Canuel et al., 2008b). Using BRET, we confirmed this interaction using Vps26A conjugated to nano-Luciferase (Vps26A-nLuc) and sortilin-YFP (Fig. 4E, black curve). As expected, the sortilin–retromer interaction was significantly weaker in Rab7A-KO cells compared with wild-type HeLa cells (Fig. 4F, red curve). We next tested the interaction in CLN3-KO HeLa cells to determine if CLN3 played a role in this interaction (Fig. 4E, blue curve). We found a significantly weakened interaction between retromer and sortilin in CLN3-KO cells compared with wild-type HeLa cells (Fig. 4F). We confirmed these BRET results using co-immunoprecipitation and found that endogenous Vps26A did not interact as efficiently with endogenous sortilin in CLN3-KO HeLa cells compared with wild-type cells (Fig. S3B).

CLN3 regulates the stability of sortilin and CI-MPR

Since we observed a weaker retromer–sortilin interaction in CLN3-KO cells and retromer is required for the efficient endosome-to-TGN trafficking of CI-MPR and sortilin (Arighi et al., 2004; Canuel et al., 2008b), we wanted to determine if lysosomal sorting receptor recycling is regulated by CLN3. In cells depleted of retromer, CI-MPR and sortilin are degraded in lysosomes rather than recycled back to the TGN (Arighi et al., 2004). We performed a cycloheximide chase experiment to determine receptor stability as we have previously done (Mamo et al., 2012; McCormick et al., 2008). Wild-type, CLN3-KO and Rab7A-KO HeLa cells were incubated with serum-free medium containing 50 µg/ml cycloheximide and collected after 0, 3, and 6 h of incubation. Western blot analysis shows decreased levels of sortilin and CI-MPR in CLN3-KO HeLa cells compared with Rab7A-KO and wild-type HeLa cells (Fig. S4A). Transfecting FLAG-CLN3 in CLN3-KO cells rescued this phenotype (Fig. S4A). Actin staining was used as a loading control, while FLAG staining was used to demonstrate the expression level of FLAG-tagged CLN3 constructs. Compared with wild-type cells, which had 92% and 88% of sortilin remaining (Fig. 5A) and 100% and 95% CI-MPR remaining (Fig. 5B) at 3 and 6 h, sortilin and CI-MPR were significantly degraded in CLN3-KO cells as they had only 30% and 19% of sortilin (Fig. 5A), and 37% and 8% of CI-MPR (Fig. 5B) remaining after 3 and 6 h. Expression of FLAG-CLN3 in CLN3-KO cells rescued the stability and hence recycling of sortilin (Fig. 5A) and CI-MPR (Fig. 5B) as they were no longer degraded and had protein levels remaining that were similar to levels in wild-type HeLa cells with 74% and 85%, and 94% and 95% remaining, respectively, at 3 and 6 h. The amount of sortilin and CI-MPR remaining in Rab7A-KO cells (89% and 85%, and 76% and 80% remaining, respectively, after 3 and 6 h) was comparable to wild-type levels (Fig. 5A,B), as although endosome-to-TGN trafficking is affected, degradation is also blocked. Next, we sought to determine the effects of CLN3 mutations known to cause human disease on the stability of these two cargo receptors. We expressed FLAG-CLN3^{R334H}, FLAG-CLN3^{V330F}, FLAG-CLN3^{E295K} and FLAG-CLN3^{L101P} in CLN3-KO HeLa cells (Fig. S4B). At 48 h post-transfection, a cycloheximide chase was performed as above and total cell lysate was collected. Western blotting with anti-FLAG antibody was used to indicate the expression level of the various expressed proteins, and anti-actin staining was used as a loading control. Although degradation of sortilin and CI-MPR was not as robust as in CLN3-KO HeLa cells, the receptors were significantly degraded in cells expressing CLN3^{V330F} (74% and 42% of sortilin and 28% and 25% of CI-MPR remaining after 3 and 6 h), CLN3^{E295K} (51% and 51% of sortilin and 57% and 31% of CI-MPR remaining after 3 and 6 h) and CLN3^{L101P} (35% and 44% of sortilin and 53% and 30% of CI-MPR remaining after 3 and 6 h) compared with wild-type cells (Fig. 5A,B). Interestingly, CLN3^{R334H} was able to rescue the phenotype (82% remaining at 3 h) for sortilin (Fig. 5A), at a level not statistically different from that in wild-type cells, but it only partially rescued sortilin degradation at 6 h (70% remaining). Expression of CLN3^{R334H} was not able to fully rescue CI-MPR (55% and 45% remaining at 3 and 6 h) (Fig. 5B). Overall, it appears that CLN3 proteins harbouring disease-causing mutations retain some function as they were able to partially rescue sortilin and CI-MPR degradation. However, they could not rescue as efficiently as wild-type CLN3, and degradation of the two lysosomal sorting receptors was significant in cells expressing CLN3 harbouring disease-causing mutations compared with wild-type cells.

Cathepsin D (also known as CTSD) is a lysosomal hydrolase whose trafficking to lysosomes is mediated by CI-MPR. Disruption of CI-MPR trafficking by depleting cells of retromer subunits or Rab7A using RNAi leads to inefficient processing of cathepsin D, resulting in the accumulation of pro and intermediate forms of the protein, and a reduction of the mature lysosomal form (Rojas et al., 2008; Seaman, 2004). Since we observed the degradation of CI-MPR and sortilin in CLN3-KO HeLa cells, we aimed to determine if this had an impact on the processing of cathepsin D (Fig. 5C). Compared with wild-type HeLa cells, which had 7.3% pro and 5.6% intermediate cathepsin D, CLN3-KO and Rab7A-KO HeLa cells had increased levels of pro-cathepsin D (28.3% and 42.3%, respectively) and intermediate cathepsin D (11.6% and 26.6%, respectively). On the other hand, CLN3-KO and Rab7A-KO HeLa cells had a reduction of mature cathepsin D (60% and 30.6%, respectively) compared with wild-type HeLa cells, which had 87% mature form (Fig. 5D).

CLN3 is required for the efficient degradation of proteins following internalization

Upon EGF stimulation, EGF receptor (EGFR) is internalized and can be either recycled to the cell surface or degraded in lysosomes (Ceresa and Peterson, 2014). Rab7A is a key regulator of the degradative pathway mediating the later steps of this process (Ceresa and Bahr, 2006; Vanlandingham and Ceresa, 2009). At least two Rab7A effectors have been implicated in EGFR degradation, RILP and PLEKHM1. Indeed, depletion of either of these proteins results in significant delays in the degradation kinetics of EGFR (Marwaha et al., 2017; McEwan et al., 2015; Progida et al., 2007). In order to determine whether CLN3 modulates this Rab7A pathway, we investigated the degradation kinetics of EGFR in wild-type, CLN3-KO and Rab7A-KO HeLa cells. Wild-type, CLN3-KO and Rab7A-KO HeLa cells were serum starved for 1 h in the presence of cycloheximide and then stimulated with 100 ng/ml EGF in the presence of cycloheximide for the indicated periods of time. The level of endogenous EGFR was determined by western blotting and anti-actin staining was used as a control (Fig. 6A). In wild-type cells, EGFR degradation was observed after 10 min and quantification of 5 independent experiments found substantial degradation at 15 (35% remaining), 30 (21% remaining) and 120 min (6% remaining) (Fig. 6B). As expected, Rab7A-KO cells had significantly delayed degradation compared with wild-type cells at most indicated time points with 82% and 76% remaining at 10 and 15 min. However, in the Rab7A-KO HeLa cells, EGFR was degraded at 30 and 120 min (Fig. 6B). When we compared the

Journal of Cell Science (2020) 133, jcs234047. doi:10.1242/jcs.234047

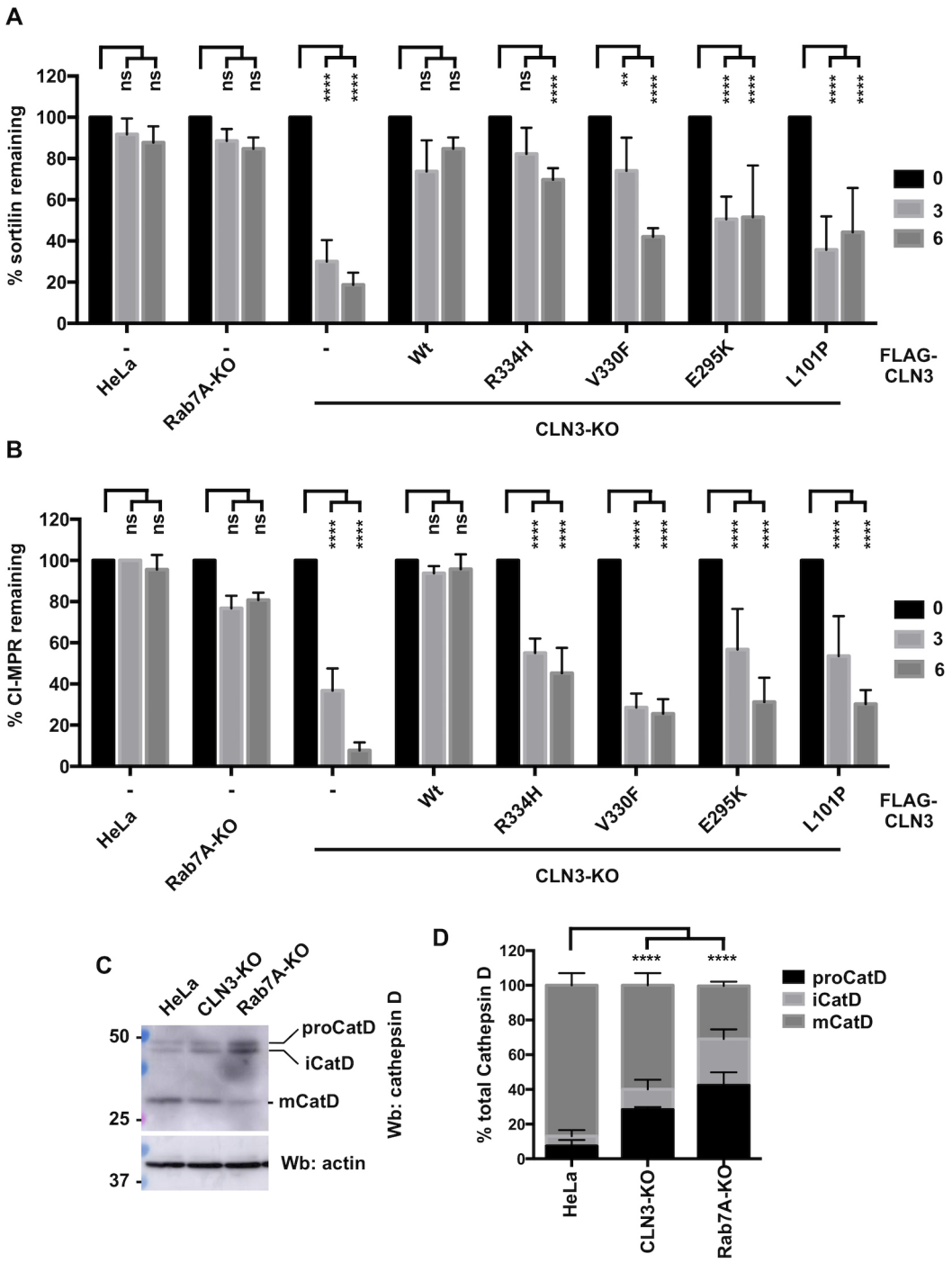

Fig. 5. CLN3 regulates the stability of sortilin and CI-MPR. (A) Wild-type, Rab7A-KO, CLN3-KO or CLN3-KO HeLa cells expressing wild-type or mutant FLAG-CLN3 as indicated, were incubated with 50 µg/ml cycloheximide in serum-free medium for 0, 3, or 6 h. Quantification of 5 separate experiments (sample blots are shown in Fig. S4) of sortilin remaining is plotted. (B) Wild-type, Rab7A-KO, CLN3-KO or CLN3-KO expressing wild-type or mutant FLAG-CLN3 as indicated were incubated with 50 µg/ml cycloheximide in serum-free media for 0, 3, or 6 h. Quantification of 5 separate experiments (sample blots are shown in Fig. S4) of CI-MPR remaining at 6 h in each group. (C) Whole cell lysate from wild-type and CLN3-KO HeLa cells was resolved by 12% SDS-PAGE. Western blotting was performed using anti-cathepsin D and anti-actin antibodies. (D) Quantification of pro-cathepsin D (proCatD, 53 kDa), intermediate cathepsin D (iCatD, 48 kDa) and mature cathepsin D (mCatD, 31 kDa). The amount of each is expressed as a percentage of total cathepsin D. Data in A, B and D are mean±s.d.; ns, not significant; $^{**}P \leq 0.01$,$^{****}P \leq 0.0001$, two-way ANOVA followed by Tukey's *post hoc* test.

degradation kinetics of EGFR in CLN3-KO cells, we found significant delays at 10 (99% remaining), 15 (97% remaining) and 30 min (77% remaining) compared with wild-type cells, with no significant difference at 120 min (Fig. 6B). The delayed degradation kinetics between Rab7A-KO and CLN3-KO was similar at 5, 10, 15 and 120 min, while the CLN3-KO cells contained significantly more EGFR at 30 min than Rab7A-KO HeLa cells.

Next, we tested the degradation kinetics of Alexa Fluor 488-labelled EGF (EGF-488) using the same cell lines to confirm our EGFR degradation result. Following 2 h of serum starvation, cells

Journal of Cell Science (2020) 133, jcs234047. doi:10.1242/jcs.234047

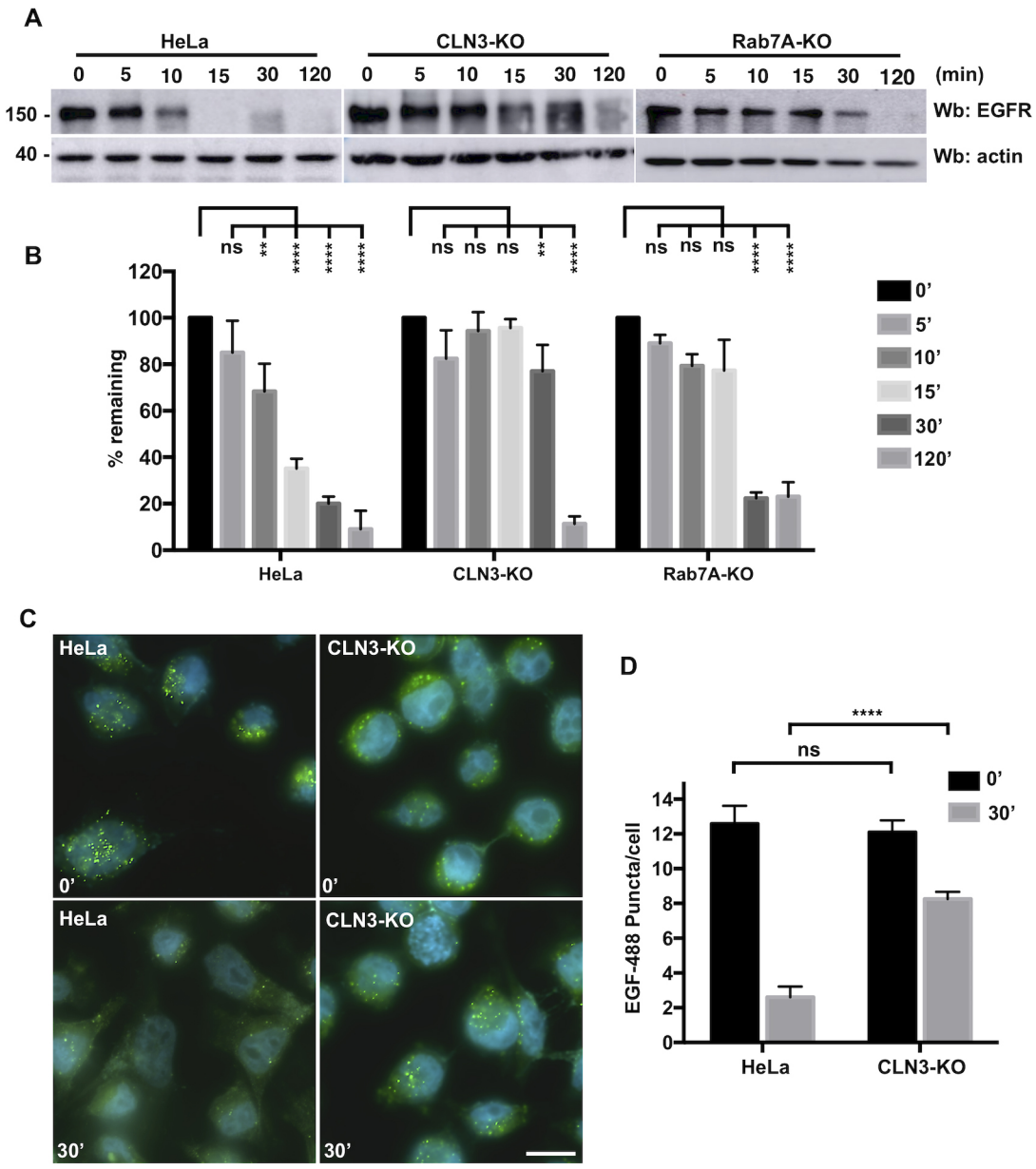

Fig. 6. CLN3 is required for EGFR degradation. (A) Wild-type, CLN3-KO and Rab7A-KO HeLa cells were incubated with 50 µg/ml cycloheximide for 1 h and subsequently treated with 100 ng/ml EGF in Opti-MEM for 0, 5, 10, 15, 30 and 120 min. Whole cell lysate was then resolved by SDS-PAGE and a western blot was performed using anti-EGFR antibody. Anti-actin staining was used as a loading control. (B) Quantification of the remaining EGFR as detected in A was performed in 5 independent experiments. (C) Wild-type and CLN3-KO HeLa cells were grown on coverslips and incubated with 300 ng/ml EGF-488 for 0 or 30 min. The cells were fixed with 4% PFA for 12 min, followed by staining with DAPI to visualize the nucleus. Images were taken on a Zeiss Fluorescence microscope using a 63× objective. (D) EGF-488 (green puncta) were counted using ImageJ in 50 cells per condition. The results shown are the average number of puncta per cell per condition. Data in B and D are mean±s.d. ns, not significant; $^{**}P \leq 0.01$, $^{****}P \leq 0.0001$; two-way ANOVA followed by Tukey's *post hoc* test. Scale bar: 10 µm.

were incubated with 300 ng/ml EGF-488 for 30 min, washed and then chased for 0 or 30 min (Fig. 6C). Images were acquired at random from the 4 different conditions and the number of EGF-488 puncta from 50 cells per condition were counted using ImageJ. At time zero, both wild-type and CLN3-KO HeLa cells had comparable numbers of EGF-488 puncta (an average of 12.57 versus 12.08, respectively). After 30 min of chase, wild-type HeLa cells had an average of 2.6 puncta per cell, whereas CLN3-KO HeLa cells had more than double this, with an average of 8.2 puncta per cell (Fig. 6D). The delayed degradation kinetics observed in the CLN3-KO cells can be explained by decreased lysosomal function as a result of defective endosome-to-TGN trafficking, or it could be that EGF and EGFR do not reach the lysosomes efficiently owing to a lack of fusion.

In order to understand the mechanism behind the delayed EGFR degradation, we used BRET to determine if the Rab7A–RILP, Rab7A–PLEKHM1 and/or Rab7A–FYCO1 interactions were affected (Fig. 7A–F). FYCO1 is a Rab7A effector required for anterograde traffic of vesicles (Pankiv et al., 2010), while RILP and PLEKHM1 are implicated in membrane fusion and degradation (Marwaha et al., 2017; McEwan et al., 2015; Progida et al., 2007). We found no significant change in the interaction between RILP and

Journal of Cell Science (2020) 133, jcs234047. doi:10.1242/jcs.234047

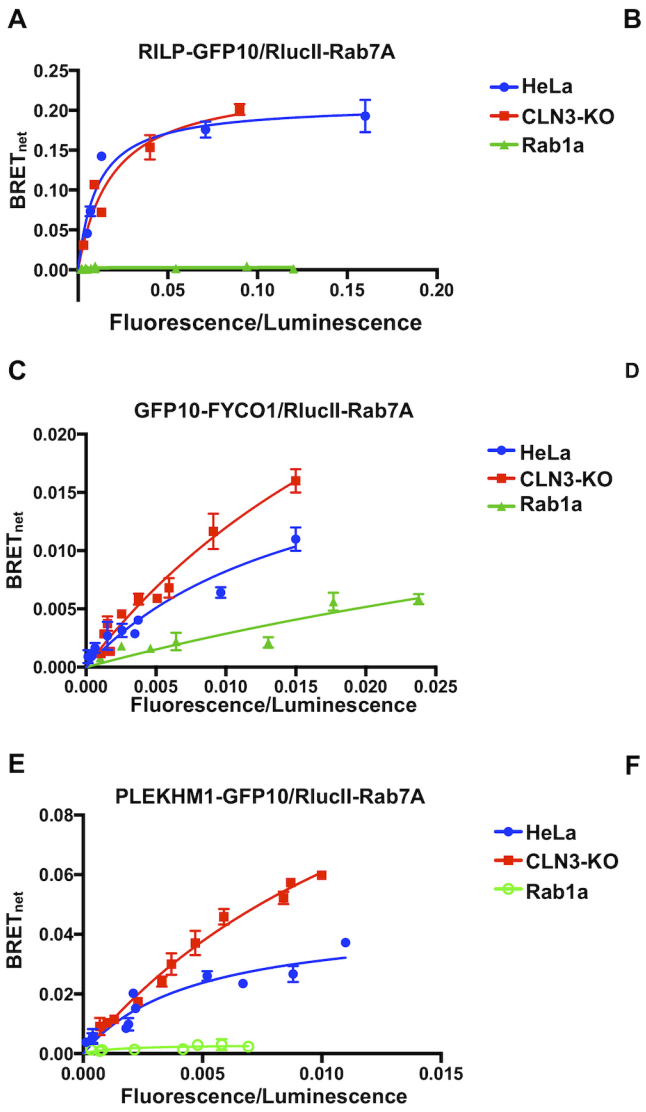

Fig. 7. CLN3 regulates endocytic degradation by modulating the Rab7A–PLEKHM1 interaction. (A) Wild-type and CLN3-KO HeLa cells were transfected with a constant amount of RlucII-Rab7A and increasing amounts of RILP-GFP10 to generate BRET titration curves. RlucII-Rab1a was also used in wild-type cells as a control. BRET signals are plotted as a function of the ratio between the GFP10 fluorescence over RlucII luminescence. (B) BRET50 was extrapolated from 3 independent experiments. (C) Wild-type and CLN3-KO HeLa cells were transfected with a constant amount of RlucII-Rab7A and increasing amounts of GFP10-FYCO1 to generate BRET titration curves. RlucII-Rab1a was also used in wild-type cells as a control. BRET signals are plotted as a function of the ratio between the GFP10 fluorescence over RlucII luminescence. (D) BRET50 was extrapolated from 3 independent experiments. (E) Wild-type and CLN3-KO HeLa cells were transfected with a constant amount of RlucII-Rab7A and increasing amounts of PLEKHM1-GFP10 to generate BRET titration curves. RlucII-Rab1a was also used in wild-type cells as a control. BRET signals are plotted as a function of the ratio between the GFP10 fluorescence over RlucII luminescence. (F) BRET50 was extrapolated from 3 independent experiments. Data in B, D and F are mean±s.d.; ns, not significant; $^{**}P \leq 0.01$; Student's *t*-test.

Rab7A (Fig. 7A,B) or FYCO1 and Rab7A (Fig. 7C,D) in either wild-type or CLN3-KO HeLa cells as shown by the $BRET_{50}$ values. We did find a change in the interaction between PLEKHM1 and Rab7A, as the $BRET_{50}$ value was 3.5-fold higher for the Rab7A–PLEKHM1 interaction in CLN3-KO cells compared with wild-type cells, suggesting a weaker interaction (Fig. 7E,F). As a control, we tested if Rab1a could interact with the Rab7A effectors above. Rab1a did not interact with any of the Rab7A effectors (Fig. 7A,C,E, green line).

DISCUSSION

CLN3 is an integral membrane protein localized to endosomes and lysosomes whose function has been implicated in intracellular trafficking and autophagy (Chandrachud et al., 2015; Metcalf et al., 2008; Oetjen et al., 2016). Previous work using *in vitro* techniques had demonstrated an interaction between CLN3 and the small GTPase Rab7A (Uusi-Rauva et al., 2012). We confirmed this interaction using BRET in live cells. Furthermore, we showed that two CLN3 mutations, $CLN3^{R334H}$ and $CLN3^{V330F}$, increased this interaction. This suggests that these two mutations could retain Rab7A on membranes longer or prevent its efficient cycling, a process required for optimal function. Interestingly, two other point mutations, $CLN3^{E295K}$ and $CLN3^{L101P}$, had no effect on this interaction. However, these two mutations weakened the CLN3–sortilin interaction. Combined with CLN3 being required for both the Rab7A–retromer and retromer–sortilin interactions, our data reveal a role for CLN3 in modulating retromer function.

It is well established that defects in retromer function or sortilin affect cathepsin D sorting and processing (Arighi et al., 2004; Canuel et al., 2008a). A previous publication demonstrated defects in the trafficking and processing of the lysosomal enzyme cathepsin D in $CLN3^{\Delta ex7–8}$/$CLN3^{\Delta ex7–8}$ cells (Fossale et al., 2004). Ablation of CLN3 results in the lysosomal degradation of sortilin and CI-MPR, which is most likely due to deficient endosome-to-TGN trafficking of sortilin and CI-MPR. Furthermore, a recently published study using proteomics to determine the impact of CLN3 mutations on lysosomal content found a decrease in 28 lysosomal proteins, including cathepsin D and prosaposin (Schmidtke et al., 2019). While the trafficking of cathepsin D to lysosomes is mediated by CI-MPR, prosaposin requires sortilin (Lefrancois et al., 2003). Combined, CLN3 appears to play a crucial role in regulating lysosomal sorting and trafficking. As such, our results provide a molecular explanation to those previous observations.

Rab7A also plays a crucial role in the degradation of endocytic cargo such as EGFR (Vanlandingham and Ceresa, 2009). We found significant delays in the degradation of both EGFR and EGF in CLN3-KO cells. This could be explained in two ways. First, CLN3 is involved in the trafficking of the lysosomal sorting receptor sortilin. Defects in trafficking of this protein, or defects in retromer function have been shown to have a significant impact on lysosome function (Arighi et al., 2004; Lefrancois et al., 2003; Seaman, 2004). Second, Rab7A is required for the fusion of endosomes and lysosomes, a process requiring RILP and PLEKHM1 (Marwaha et al., 2017; McEwan et al., 2015; Progida et al., 2007). Although we found no change in the Rab7A–RILP interaction in CLN3-KO cells, we found a significant decrease in the Rab7A–PLEKHM1 interaction. This suggests defective fusion events. Combined with decreased lysosomal function, this could explain the significant delay in EGF and EGFR degradation. The Akt–mTOR pathway is upregulated in JNCL patient fibroblasts (Vidal-Donet et al., 2013). EGFR is known to activate several signalling pathways, including Akt (Mattoon et al., 2004). Dysregulated trafficking and degradation of EGFR can lead to increased signalling (Sorkin and von Zastrow, 2009). Our results could at least partially explain the upregulation of the Akt–mTOR pathway found in JNCL patient fibroblasts.

Autophagy is affected in CLN3-deficient cells (Chandrachud et al., 2015; Chang et al., 2011; Vidal-Donet et al., 2013). Our CLN3-KO HeLa cells also show defective autophagy, similar to the defects observed in the Rab7A-KO. This suggests defects late in the autophagy pathway, possibly at the fusion step with lysosomes. PLEKHM1, among other factors, plays a critical role in modulating autophagosome fusion with lysosomes (McEwan et al., 2015). Defects in this fusion machinery lead- to defective autophagy, but also delayed EGFR degradation kinetics. We propose that defects in autophagy observed in patients with JNCL could be due to defects in PLEKHM1 function, along with defects in lysosome function due to decreased sorting of sortilin and CI-MPR.

In conclusion, our results point to a role of CLN3 in the regulation of a subset of Rab7A functions. We have previously shown a similar role for CLN5, a soluble protein found within the lumen of endosomes and lysosomes (Mamo et al., 2012). As CLN3 and CLN5 are known to interact, we speculate that the two proteins could function as a complex to regulate Rab7A and retromer function, demonstrating, at least partially, the molecular mechanisms deficient in JNCL.

MATERIALS AND METHODS

Plasmids and mutagenesis

RlucII-CLN3 and GFP10-CLN3 were generated by amplifying *CLN3* cDNA from FLAG-CLN3 (EX-Q0362-M12, Genecopoeia, Rockville, MD) and cloned into the EcoRV-XhoI and EcoRV-XbaI sites of pcDNA3.1Hygro(+)RlucII-GFP10-st2 and pcDNA3.1Hygro(+)GFP10-RlucII-st2 plasmids, respectively (a gift from Michel Bouvier, University de Montreal). To generate Vps26A-nLuc, Vps26A cDNA was obtained by PCR from Vps26A-YFP plasmid. pnLuc-N1 was generated by replacing the eYFP of pEYFP-N1 with nano-Luc (a gift from Regis Grailhe, Pasteur Institute Korea). Cloning was done after digestion of pnLuc-N1 plasmid with XhoI-HindIII restriction enzymes. PLEKHM1-GFP10 was engineered by inserting PLEKHM1 (Addgene plasmid #73592, deposited by Paul Odgren) into the NheI-EcoRV sites of pcDNA3.1 Hygro (+) GFP10-RLucII-st2. To generate GFP10-FYCOI, cDNA of FYCOI was obtained by PCR from mCherry-FYCOI (a gift from John H. Brumell, Sickkids Hospital) and cloned into the KpnI-XbaI sites of pcDNA3.1 Hygro (+) GFP10-RLucII. The various mutants were engineered using site-directed mutagenesis from the previously described FLAG-CLN3, GFP10-CLN3, RlucII-CLN3 constructs. Sortilin-YFP was a gift from Makoto Kanzaki, Tohoku University. Raichu-Rab7A was a gift from Takeshi Nakamura, Tokyo University of Science. RlucII-Rab7A, RlucII-Rab1a, Vps26A-GFP10 and RILP-GFP10 were previously described (Modica et al., 2017).

Antibodies

The following mouse monoclonal antibodies were used: anti-actin (WB: 1:3000, BD Biosciences, 612657); anti-α-tubulin (WB: 1:1000, Sigma-Aldrich, T9026); anti-Lamp1 (WB: 1:500, Abcam ab25631); anti-CI-MPR (WB: 1 µg/ml, Serotec, MCA2048); anti-Cathepsin D (WB: 1:100, Sigma-Aldrich, IM03). The following rabbit monoclonal antibodies were used: anti-Rab7A (WB: 1:1000, Cell Signaling Technology D95F2); anti-EGFR (WB: 1:1000, Abcam ab52894); anti-LC3 (WB: 1:2000, Abcam ab192890). The following rabbit polyclonal antibodies were used: anti-Vps26A (WB: 1:2000, Abcam ab23892); anti-RILP (WB: 1:1000, Abcam ab128616); anti-FLAG (WB: 1:1000, Sigma-Aldrich F7425); anti-sortilin (WB: 1 µg/ml, Abcam ab16640). The following goat polyclonal antibody was used: anti-Vps35 (WB: 1:000, Novus Biologicals NB1001397).

Cell culture and transient transfections

HeLa cells were cultured in Dulbecco's modified Eagle's medium (DMEM) supplemented with 2 mM L-glutamine, 100 U/ml penicillin, 100 g/ml streptomycin and 10% FBS (Thermo Fisher Scientific, Burlington, ON) at 37°C in a humidified chamber at 95% air and 5% CO_2. Cells were seeded at a density of 2×10^5/well for 12-well plates and 5×10^5/well for 6-well plates 24 h prior to transfection. Transfections were performed with polyethylenimine (PEI) (Thermo Fisher Scientific). Briefly, solution 1 was prepared by diluting plasmid into Opti-MEM (Thermo Fisher Scientific). Solution 2 was prepared by diluting PEI (1 µg/µl) in Opti-MEM in a 1:3 ratio with the DNA to be transfected. After a 5 min incubation, the two solutions were mixed, vortexed for 3 s, incubated at room temperature (RT) for 15 min and added to the cells.

CRISPR/Cas9 editing

In order to generate CLN3-knockout cells, a guide RNA (gRNA) corresponding to the first exon of *CLN3* was designed (CACCGCGGCG-CTTTTCGGATTCCGA) and cloned into pX330-U6 expressing a humanized Cas9 (Cong et al., 2013). HeLa cells were co-transfected with pX330-U6-gRNA-CLN3 and pcDNA3.1-zeocin (Thermo Fisher Scientific). 24 h after transfection, cells were selected with zeocin (250 µg/ml) for 5 days. Cells were cultured for 2 weeks, single clones were isolated and genomic DNA extracted. DNA sequencing was performed to identify CLN3-knockout cells carrying a specific indel mutation. HeLa cells were transfected with an all-in-one CRISPR/Cas9 plasmid for Rab7A (plasmid number HTN218819, Genecopoeia, Rockville, MD). 72 h post-transfection, the cells were treated with 1 mg/ml geneticin (Thermo Fisher Scientific) for 1 week. Limited dilution was performed to isolate single cells which were allowed to grow for 2 weeks. Western blotting was used to identify Rab7A-KO cells.

BRET titration experiments

HeLa cells were seeded in 12-well plates and transfected with the indicated plasmids. 48 h post-transfection, cells were washed in PBS, detached with 5 mM EDTA in PBS and collected in 500 µl PBS. Cells were transferred to opaque 96-well plates (VWR Canada, Mississauga, ON) in triplicate. Total fluorescence was first measured with the Tecan Infinite M1000 Pro plate reader (Tecan Group Ltd., Mannedorf, Switzerland) with the excitation and emission set at 400 nm and 510 nm, respectively, for $BRET^2$ and 500 nm and 530 nm for $BRET^1$. The $BRET^2$ substrate coelenterazine 400a and $BRET^1$ substrate h-coelenterazine were then added to all wells (5 µM final concentration) and the $BRET^2$ and $BRET^1$ signals were measured 2 min later. The BRET signals were calculated as a ratio of the light emitted at 525±15 nm over the light emitted at 410±40 nm. The BRETnet signals were calculated as the difference between the BRET signal in cells expressing both fluorescence and luminescence constructs and the BRET signal from cells where only the luminescence fused construct was expressed.

Western blotting

Cells were detached using 5 mM EDTA in PBS, washed in 1× PBS and collected by centrifugation. TNE buffer (150 mM NaCl, 50 mM Tris-HCl, pH 7.5, 2 mM EDTA, 0.5% Triton X-100 and protease inhibitor cocktail) was used to lyse cells by incubating them for 30 min on ice. Lysates were centrifuged at high speed for 10 min and the supernatants (cell lysate) were collected to be analyzed by western blotting. Samples were mixed with sample buffer 3× to obtain a final concentration of 1× (62.5 mM Tris-HCl, pH 6.5, 2.5% SDS, 10% glycerol, 0.01% Bromophenol Blue). Prior to electrophoresis, samples were incubated at 95°C for 5 min and resolved on SDS-PAGE followed by wet-transfer to nitrocellulose membranes. Detection was done by immunoblotting using the indicated antibodies.

Membrane separation assay

24 h post-transfection, cells were collected in 5 mM EDTA in PBS. The cells were subsequently snap frozen in liquid nitrogen and allowed to thaw at room temperature for 5 min. The cells were resuspended in Buffer 1 (0.1 M Mes-NaOH, pH 6.5, 1 mM magnesium acetate, 0.5 mM EGTA, 200 M sodium orthovanadate, 0.2 M sucrose) and centrifuged at 10,000 ***g*** for 5 min at 4°C. The supernatant containing the cytosolic proteins (S, soluble fraction) was collected. The remaining pellet was resuspended in Buffer 2 (50 mM Tris-HCl, 150 mM NaCl, 1 mM EDTA, 0.1% SDS, 1% Triton X-100) and centrifuged at 10,000 ***g*** for 5 min at 4°C. Samples were loaded into SDS-PAGE gels in equal volumes. Fiji was used to quantify the intensity of the bands (Schindelin et al., 2012). The intensity of each fraction was calculated and divided by the total intensity to determine the distribution of proteins.

Cycloheximide chase

Wild-type, CLN3-KO, Rab7A-KO HeLa cells were seeded in 6-well plates the day prior to transfection. 500 ng of FLAG fused wild-type and mutation harbouring CLN3 was transfected into CLN3-KO HeLa cells. 48 h after transfection, cells were treated with 50 µg/ml of cycloheximide in Opti-MEM. Lysates were collected at 0, 3 or 6 h time points and run on 10% SDS-PAGE gels. Fiji was used to quantify the intensity of the bands (Schindelin et al., 2012). All protein levels were standardized to the actin loading control. Amount of remaining protein is expressed as a percentage of the 0 time point in each group.

EGFR degradation assay

Wild-type, CLN3-KO and Rab7A-KO cells were seeded in 6-well plates the day before the assay. In order to prevent *de novo* synthesis EGFR during EGF stimulation, cells were treated with 50 µg/ml cycloheximide in Opti-MEM for 1 h. EGF stimulation was performed with 100 ng/ml EGF in Opti-MEM containing 50 µg/ml of cycloheximide. Cell lysates were collected as indicated above and western blotting was performed. Fiji was used to quantify the intensity of the bands (Schindelin et al., 2012). All protein levels were standardized to the actin loading control. Amount of remaining protein is expressed as a percentage of the 0 time point in each group.

EGF-488 pulse-chase

Wild-type and CLN3-KO HeLa cells were seeded on coverslips the day before the experiment. Cells were serum starved in Opti-MEM for 1 h followed by a 30-min pulse of 300 ng/ml of EGF-488. Cells were then washed with PBS, fixed in 4% paraformaldehyde at 0 and 30 min and mounted onto slide using Fluoromount-G (Thermo Fisher). The coverslips were sealed using nail polish. Cells were imaged using fluorescence microscope. The number of puncta per cell was counted using Fiji. Briefly, the images were split into their individual channels. Using the green channel, the threshold was adjusted to 0.93% in order to get signal only from the puncta. The number of puncta counted from an image was divided by the number of nuclei within that image, which gave us the number of puncta per cell. 50 cells per condition for each time point were analyzed.

Autophagic flux

Wild-type, CLN3-KO, Rab7A-KO HeLa cells were seeded in 6-well plates the day before autophagy induction. Cells were starved with Earle's balanced salt solution (EBSS) for 4 h to induce autophagy. 100 nM Bafilomycin A1 (BafA1) was used to inhibit lysosomal function and therefore inhibit autophagy. Lysates were resolved by SDS-PAGE and blotted with anti-LC3 and anti-actin antibodies. Band intensity was determined using Fiji, and quantification was performed as LC3-II over LC3-I+LC3-II.

Acyl-RAC to isolate palmitoylated proteins

The protocol to detect palmitoylated protein was adapted from a published protocol (Ren et al., 2013). Briefly, protein lysates were incubated overnight at room temperature with 0.5% methyl methanethiosulfonate (MMTS) (Sigma-Aldrich) to block free cysteine residues. Proteins were then precipitated by adding two volumes of cold acetone and incubated at −20°C for 2 h. After washing with cold acetone, the pellet was resuspended in binding buffer (100 mM HEPES, 1 mM EDTA, 1% SDS). Water-swollen thiopropyl Sepharose 6B (GE Healthcare Life Sciences) was added and samples were divided into two equal parts. One part was treated with hydroxylamine (Sigma-Aldrich), pH 7.5, to a final concentration of 0.2 M to cleave palmitate residues from proteins; the other part was treated with an equal amount of NaCl as a control. After 3 h incubation at room temperature, beads were washed five times with binding buffer and captured proteins were eluted with 75 mM dithiothreitol.

Raichu-Rab7A FRET sensor

Wild-type or CLN3-KO HeLa cells were seeded in 12-well plates and transfected with the Raichu-Rab7A sensor. 36 h post-transfection, cells were washed in PBS, detached with 5 mM EDTA in PBS and collected in 500 µl PBS. Cells were transferred to white opaque 96-well plates (VWR Canada, Mississauga, ON) in triplicate. After excitation at 433 nm, the light emitted at the maximal emission of CFP (475 nm) and Ypet (525 nm) was measured on a Tecan Infinite M1000 Pro plate reader (Tecan Group Ltd., Mannedorf, Switzerland). Data are presented as a ratio of the light emitted at 525 nm (Ypet) divided by the light emitted at 475 nm (CFP).

Statistics

Statistical analysis was performed using GraphPad Prism v.7. The statistical tests used are described in the respective figure legends.

Acknowledgements

We would like to thank Michel Bouvier (IRIC and University de Montreal), Regis Grailhe (Pasteur Institute Korea), Paul Odgren (University of Massachusetts Medical School), Makoto Kanzaki (Tohoku University) and Takeshi Nakamura (Tokyo University of Science) for providing plasmids.

Competing interests

The authors declare no competing or financial interests.

Author contributions

Conceptualization: S.Y., G.M., E.S., G.H., S.L.; Methodology: S.Y., G.M., E.S., A.K., G.H., S.L.; Validation: G.H., S.L.; Formal analysis: S.Y., G.M., E.S., A.K., S.L.; Investigation: S.Y., G.M., E.S., A.K.; Resources: A.K.; Writing - original draft: S.Y., S.L.; Writing - review & editing: S.Y., G.M., E.S., G.H., S.L.; Supervision: G.H., S.L.; Project administration: S.L.; Funding acquisition: G.H., S.L.

Funding

This work was supported by an EU Joint Programme in Neurodegenerative Diseases Grant (Neuronode to S.L.), the Canadian Institutes for Health Research (ENG-387575 to S.L.), the Canadian Foundation for Innovation (35258 to S.L.), the National Contest for Life Foundation Germany (NCL) (to G.H.) and by the Deutsche Forschungsgemeinschaft (DFG; 425373668, HE 3220/4-1 to G.H.). S.Y. is supported by a Fondation Universitaire Armand-Frappier scholarship. G.M. is supported by a scholarship from Fond de Recherche du Quebec - Santé.

Supplementary information

Supplementary information available online at
http://jcs.biologists.org/lookup/doi/10.1242/jcs.234047.supplemental

References

Anderson, G. W., Goebel, H. H. and Simonati, A. (2012). Human pathology in NCL. *Biochim. Biophys. Acta* **1832**, 1807-1826. doi:10.1016/j.bbadis.2012.11.014

Arighi, C. N., Hartnell, L. M., Aguilar, R. C., Haft, C. R. and Bonifacino, J. S. (2004). Role of the mammalian retromer in sorting of the cation-independent

mannose 6-phosphate receptor. *J. Cell Biol.* **165**, 123-133. doi:10.1083/jcb.200312055

Barr, F. and Lambright, D. G. (2010). Rab GEFs and GAPs. *Curr. Opin. Cell Biol.* **22**, 461-470. doi:10.1016/j.ceb.2010.04.007

Canuel, M., Korkidakis, A., Konnyu, K. and Morales, C. R. (2008a). Sortilin mediates the lysosomal targeting of cathepsins D and H. *Biochem. Biophys. Res. Commun.* **373**, 292-297. doi:10.1016/j.bbrc.2008.06.021

Canuel, M., Lefrancois, S., Zeng, J. and Morales, C. R. (2008b). AP-1 and retromer play opposite roles in the trafficking of sortilin between the Golgi apparatus and the lysosomes. *Biochem. Biophys. Res. Commun.* **366**, 724-730. doi:10.1016/j.bbrc.2007.12.015

Cao, Y., Espinola, J. A., Fossale, E., Massey, A. C., Cuervo, A. M., MacDonald, M. E. and Cotman, S. L. (2006). Autophagy is disrupted in a knock-in mouse model of juvenile neuronal ceroid lipofuscinosis. *J. Biol. Chem.* **281**, 20483-20493. doi:10.1074/jbc.M602180200

Ceresa, B. P. and Bahr, S. J. (2006). rab7 activity affects epidermal growth factor: epidermal growth factor receptor degradation by regulating endocytic trafficking from the late endosome. *J. Biol. Chem.* **281**, 1099-1106. doi:10.1074/jbc.M504175200

Ceresa, B. P. and Peterson, J. L. (2014). Cell and molecular biology of epidermal growth factor receptor. *Int. Rev. Cell Mol. Biol.* **313**, 145-178. doi:10.1016/B978-0-12-800177-6.00005-0

Chandrachud, U., Walker, M. W., Simas, A. M., Heetveld, S., Petcherski, A., Klein, M., Oh, H., Wolf, P., Zhao, W.-N., Norton, S. et al. (2015). Unbiased cell-based screening in a neuronal cell model of batten disease highlights an interaction between $Ca2^+$ homeostasis, autophagy, and CLN3 protein function. *J. Biol. Chem.* **290**, 14361-14380. doi:10.1074/jbc.M114.621706

Chang, J.-W., Choi, H., Cotman, S. L. and Jung, Y.-K. (2011). Lithium rescues the impaired autophagy process in CbCln3(Deltaex7/8/Deltaex7/8) cerebellar cells and reduces neuronal vulnerability to cell death via IMPase inhibition. *J. Neurochem.* **116**, 659-668. doi:10.1111/j.1471-4159.2010.07158.x

Coelho, D., Kim, J. C., Miousse, I. R., Fung, S., du Moulin, M., Buers, I., Suormala, T., Burda, P., Frapolli, M., Stucki, M. et al. (2012). Mutations in ABCD4 cause a new inborn error of vitamin B12 metabolism. *Nat. Genet.* **44**, 1152-1155. doi:10.1038/ng.2386

Cong, L., Ran, F. A., Cox, D., Lin, S., Barretto, R., Habib, N., Hsu, P. D., Wu, X., Jiang, W., Marraffini, L. A. et al. (2013). Multiplex genome engineering using CRISPR/Cas systems. *Science* **339**, 819-823. doi:10.1126/science.1231143

Cotman, S. L. and Staropoli, J. F. (2012). The juvenile Batten disease protein, CLN3, and its role in regulating anterograde and retrograde post-Golgi trafficking. *Clin. Lipidol.* **7**, 79-91. doi:10.2217/clp.11.70

Dumaresq-Doiron, K., Savard, M.-F., Akam, S., Costantino, S. and Lefrancois, S. (2010). The phosphatidylinositol 4-kinase PI4KIIIalpha is required for the recruitment of GBF1 to Golgi membranes. *J. Cell Sci.* **123**, 2273-2280. doi:10.1242/jcs.055798

Fossale, E., Wolf, P., Espinola, J. A., Lubicz-Nawrocka, T., Teed, A. M., Gao, H., Rigamonti, D., Cattaneo, E., MacDonald, M. E. and Cotman, S. L. (2004). Membrane trafficking and mitochondrial abnormalities precede subunit c deposition in a cerebellar cell model of juvenile neuronal ceroid lipofuscinosis. *BMC Neurosci.* **5**, 57. doi:10.1186/1471-2202-5-57

Ganley, I. G., Wong, P.-M., Gammoh, N. and Jiang, X. (2011). Distinct autophagosomal-lysosomal fusion mechanism revealed by thapsigargin-induced autophagy arrest. *Mol. Cell* **42**, 731-743. doi:10.1016/j.molcel.2011.04.024

Grosshans, B. L., Ortiz, D. and Novick, P. (2006). Rabs and their effectors: achieving specificity in membrane traffic. *Proc. Natl. Acad. Sci. USA* **103**, 11821-11827. doi:10.1073/pnas.0601617103

Haskell, R. E., Carr, C. J., Pearce, D. A., Bennett, M. J. and Davidson, B. L. (2000). Batten disease: evaluation of CLN3 mutations on protein localization and function. *Hum. Mol. Genet.* **9**, 735-744. doi:10.1093/hmg/9.5.735

Hutagalung, A. H. and Novick, P. J. (2011). Role of Rab GTPases in membrane traffic and cell physiology. *Physiol. Rev.* **91**, 119-149. doi:10.1152/physrev.00059.2009

Kobayashi, H., Ogawa, K., Yao, R., Lichtarge, O. and Bouvier, M. (2009). Functional rescue of beta-adrenoceptor dimerization and trafficking by pharmacological chaperones. *Traffic* **10**, 1019-1033. doi:10.1111/j.1600-0854.2009.00932.x

Lefrancois, S., Zeng, J., Hassan, A. J., Canuel, M. and Morales, C. R. (2003). The lysosomal trafficking of sphingolipid activator proteins (SAPs) is mediated by sortilin. *EMBO J.* **22**, 6430-6437. doi:10.1093/emboj/cdg629

Lojewski, X., Staropoli, J. F., Biswas-Legrand, S., Simas, A. M., Haliw, L., Selig, M. K., Coppel, S. H., Goss, K. A., Petcherski, A., Chandrachud, U. et al. (2014). Human iPSC models of neuronal ceroid lipofuscinosis capture distinct effects of TPP1 and CLN3 mutations on the endocytic pathway. *Hum. Mol. Genet.* **23**, 2005-2022. doi:10.1093/hmg/ddt596

Luiro, K., Yliannala, K., Ahtiainen, L., Maunu, H., Järvelä, I., Kyttälä, A. and Jalanko, A. (2004). Interconnections of CLN3, Hook1 and Rab proteins link Batten disease to defects in the endocytic pathway. *Hum. Mol. Genet.* **13**, 3017-3027. doi:10.1093/hmg/ddh321

Mamo, A., Jules, F., Dumaresq-Doiron, K., Costantino, S. and Lefrancois, S. (2012). The role of ceroid lipofuscinosis neuronal protein 5 (CLN5) in endosomal sorting. *Mol. Cell. Biol.* **32**, 1855-1866. doi:10.1128/MCB.06726-11

Marwaha, R., Arya, S. B., Jagga, D., Kaur, H., Tuli, A. and Sharma, M. (2017). The Rab7 effector PLEKHM1 binds Arl8b to promote cargo traffic to lysosomes. *J. Cell Biol.* **216**, 1051-1070. doi:10.1083/jcb.201607085

Mattoon, D. R., Lamothe, B., Lax, I. and Schlessinger, J. (2004). The docking protein Gab1 is the primary mediator of EGF-stimulated activation of the PI-3K/Akt cell survival pathway. *BMC Biol.* **2**, 24. doi:10.1186/1741-7007-2-24

McCormick, P. J., Dumaresq-Doiron, K., Pluviose, A.-S., Pichette, V., Tosato, G. and Lefrancois, S. (2008). Palmitoylation controls recycling in lysosomal sorting and trafficking. *Traffic* **9**, 1984-1997. doi:10.1111/j.1600-0854.2008.00814.x

McEwan, D. G., Popovic, D., Gubas, A., Terawaki, S., Suzuki, H., Stadel, D., Coxon, F. P., Miranda de Stegmann, D., Bhogaraju, S., Maddi, K. et al. (2015). PLEKHM1 regulates autophagosome-lysosome fusion through HOPS complex and LC3/GABARAP proteins. *Mol. Cell* **57**, 39-54. doi:10.1016/j.molcel.2014.11.006

Mercier, J.-F., Salahpour, A., Angers, S., Breit, A. and Bouvier, M. (2002). Quantitative assessment of $beta_1$- and $beta_2$-adrenergic receptor homo- and heterodimerization by bioluminescence resonance energy transfer. *J. Biol. Chem.* **277**, 44925-44931. doi:10.1074/jbc.M205767200

Metcalf, D. J., Calvi, A. A., Seaman, M. N. J., Mitchison, H. M. and Cutler, D. F. (2008). Loss of the Batten disease gene CLN3 prevents exit from the TGN of the mannose 6-phosphate receptor. *Traffic* **9**, 1905-1914. doi:10.1111/j.1600-0854.2008.00807.x

Modica, G., Skorobogata, O., Sauvageau, E., Vissa, A., Yip, C. M., Kim, P. K., Wurtele, H. and Lefrancois, S. (2017). Rab7 palmitoylation is required for efficient endosome-to-TGN trafficking. *J. Cell Sci.* **130**, 2579-2590. doi:10.1242/jcs.199729

Mole, S. E. and Cotman, S. L. (2015). Genetics of the neuronal ceroid lipofuscinoses (Batten disease). *Biochim. Biophys. Acta* **1852**, 2237-2241. doi:10.1016/j.bbadis.2015.05.011

Oetjen, S., Kuhl, D. and Hermey, G. (2016). Revisiting the neuronal localization and trafficking of CLN3 in juvenile neuronal ceroid lipofuscinosis. *J. Neurochem.* **139**, 456-470. doi:10.1111/jnc.13744

Pankiv, S., Alemu, E. A., Brech, A., Bruun, J.-A., Lamark, T., Øvervatn, A., Bjørkøy, G. and Johansen, T. (2010). FYCO1 is a Rab7 effector that binds to LC3 and PI3P to mediate microtubule plus end-directed vesicle transport. *J. Cell Biol.* **188**, 253-269. doi:10.1083/jcb.200907015

Pfeffer, S. and Aivazian, D. (2004). Targeting Rab GTPases to distinct membrane compartments. *Nat. Rev. Mol. Cell Biol.* **5**, 886-896. doi:10.1038/nrm1500

Prause, J., Goswami, A., Katona, I., Roos, A., Schnizler, M., Bushuven, E., Dreier, A., Buchkremer, S., Johann, S., Beyer, C. et al. (2013). Altered localization, abnormal modification and loss of function of sigma receptor-1 in amyotrophic lateral sclerosis. *Hum. Mol. Genet.* **22**, 1581-1600. doi:10.1093/hmg/ddt008

Progida, C., Malerod, L., Stuffers, S., Brech, A., Bucci, C. and Stenmark, H. (2007). RILP is required for the proper morphology and function of late endosomes. *J. Cell Sci.* **120**, 3729-3737. doi:10.1242/jcs.017301

Ratajczak, E., Petcherski, A., Ramos-Moreno, J. and Ruonala, M. O. (2014). FRET-assisted determination of CLN3 membrane topology. *PLoS ONE* **9**, e102593. doi:10.1371/journal.pone.0102593

Ren, W., Jhala, U. S. and Du, K. (2013). Proteomic analysis of protein palmitoylation in adipocytes. *Adipocyte* **2**, 17-28. doi:10.4161/adip.22117

Rojas, R., van Vlijmen, T., Mardones, G. A., Prabhu, Y., Rojas, A. L., Mohammed, S., Heck, A. J. R., Raposo, G., van der Sluijs, P. and Bonifacino, J. S. (2008). Regulation of retromer recruitment to endosomes by sequential action of Rab5 and Rab7. *J. Cell Biol.* **183**, 513-526. doi:10.1083/jcb.200804048

Schindelin, J., Arganda-Carreras, I., Frise, E., Kaynig, V., Longair, M., Pietzsch, T., Preibisch, S., Rueden, C., Saalfeld, S., Schmid, B. et al. (2012). Fiji: an open-source platform for biological-image analysis. *Nat. Methods* **9**, 676-682. doi:10.1038/nmeth.2019

Schmidtke, C., Tiede, S., Thelen, M., Käkelä, R., Jabs, S., Makrypidi, G., Sylvester, M., Schweizer, M., Braren, I., Brocke-Ahmadinejad, N. et al. (2019). Lysosomal proteome analysis reveals that CLN3-defective cells have multiple enzyme deficiencies associated with changes in intracellular trafficking. *J. Biol. Chem.* **294**, 9592-9604. doi:10.1074/jbc.RA119.008852

Seaman, M. N. J. (2004). Cargo-selective endosomal sorting for retrieval to the Golgi requires retromer. *J. Cell Biol.* **165**, 111-122. doi:10.1083/jcb.200312034

Seaman, M. N. J., Harbour, M. E., Tattersall, D., Read, E. and Bright, N. (2009). Membrane recruitment of the cargo-selective retromer subcomplex is catalysed by the small GTPase Rab7 and inhibited by the Rab-GAP TBC1D5. *J. Cell Sci.* **122**, 2371-2382. doi:10.1242/jcs.048686

Sorkin, A. and von Zastrow, M. (2009). Endocytosis and signalling: intertwining molecular networks. *Nat. Rev. Mol. Cell Biol.* **10**, 609-622. doi:10.1038/nrm2748

Storch, S., Pohl, S. and Braulke, T. (2004). A dileucine motif and a cluster of acidic amino acids in the second cytoplasmic domain of the batten disease-related CLN3 protein are required for efficient lysosomal targeting. *J. Biol. Chem.* **279**, 53625-53634. doi:10.1074/jbc.M410930200

Uusi-Rauva, K., Kyttälä, A., van der Kant, R., Vesa, J., Tanhuanpää, K., Neefjes, J., Olkkonen, V. M. and Jalanko, A. (2012). Neuronal ceroid lipofuscinosis protein CLN3 interacts with motor proteins and modifies location of late endosomal compartments. *Cell. Mol. Life Sci.* **69**, 2075-2089. doi:10.1007/s00018-011-0913-1

Vanlandingham, P. A. and Ceresa, B. P. (2009). Rab7 regulates late endocytic trafficking downstream of multivesicular body biogenesis and cargo sequestration. *J. Biol. Chem.* **284**, 12110-12124. doi:10.1074/jbc.M809277200

Vesa, J., Chin, M. H., Oelgeschläger, K., Isosomppi, J., DellAngelica, E. C., Jalanko, A. and Peltonen, L. (2002). Neuronal ceroid lipofuscinoses are connected at molecular level: interaction of CLN5 protein with CLN2 and CLN3. *Mol. Biol. Cell* **13**, 2410-2420. doi:10.1091/mbc.e02-01-0031

Vidal-Donet, J. M., Cárcel-Trullols, J., Casanova, B., Aguado, C. and Knecht, E. (2013). Alterations in ROS activity and lysosomal pH account for distinct patterns of macroautophagy in LINCL and JNCL fibroblasts. *PLoS ONE* **8**, e55526. doi:10.1371/journal.pone.0055526

Wijdeven, R. H., Janssen, H., Nahidiazar, L., Janssen, L., Jalink, K., Berlin, I. and Neefjes, J. (2016). Cholesterol and ORP1L-mediated ER contact sites control autophagosome transport and fusion with the endocytic pathway. *Nat. Commun.* **7**, 11808. doi:10.1038/ncomms11808

Yasuda, S., Morishita, S., Fujita, A., Nanao, T., Wada, N., Waguri, S., Schiavo, G., Fukuda, M. and Nakamura, T. (2016). Mon1-Ccz1 activates Rab7 only on late endosomes and dissociates from the lysosome in mammalian cells. *J. Cell Sci.* **129**, 329-340. doi:10.1242/jcs.178095